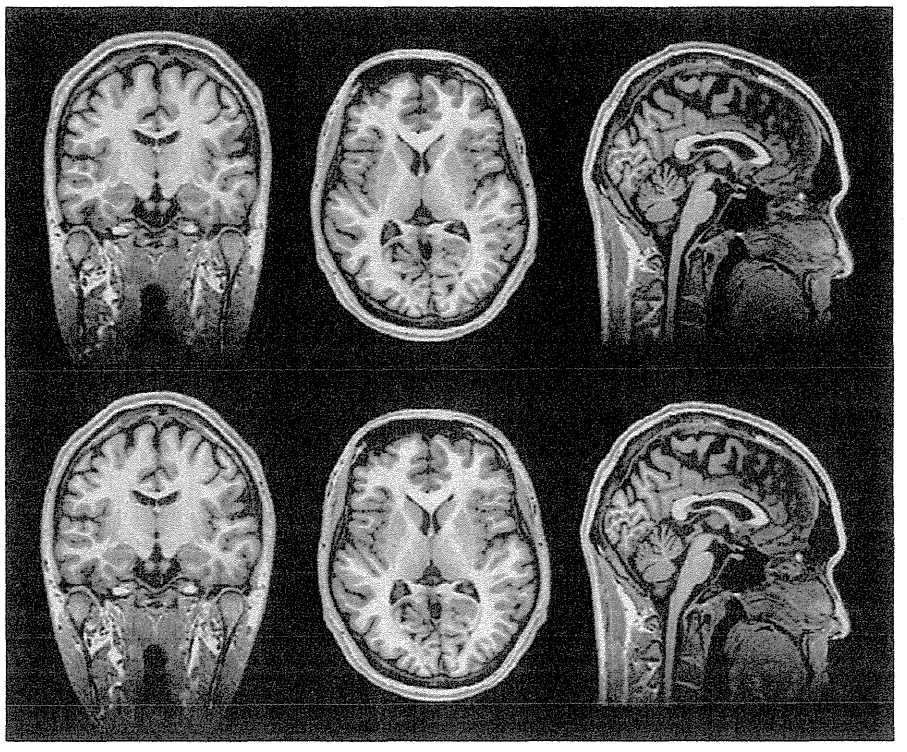

Fig. 5. Upper side, T_1W-weighted imaging (T_1WI) with spherical harmonics description of gradients (SHDG) correction; lower side, T_1WI without SHDG correction of a subject in the present study. Figure shows representative coronal, axial, and saggital slices of the original structural T_1 volume.

tion correction more accurately estimated brain volume. However, in their phantom study, Jovicich's group showed that the phantom volume from a corrected image was much closer to the true phantom volume.[8] We performed a similar inspection and obtained a similar result. Therefore, we can conclude that VBM analysis using a corrected image provides a result near to the true brain volume.

Conclusions

We believe this is the first VBM study to show that the use of corrected images can reduce volumetric errors caused by system variations. These results indicate that correction of distortion induced by gradient nonlinearity is mandatory in multi-scanner or multi-site imaging trials.

Acknowledgments

This study was supported by grants-in-aid for Comprehensive Research on Aging and Health from the Ministry of Health, Labor and Welfare, Japan.

References

1. Ashburner J, Friston KJ. Voxel-based morphometry—the methods. Neuroimage 2000; 11:805–821.
2. Good CD, Johnsrude I, Ashburner J, Henson RN, Friston KJ, Frackowiak RS. Cerebral asymmetry and the effects of sex and handedness on brain structure: a voxel-based morphometric analysis of 465 normal adult human brains. Neuroimage 2001; 14:685–700.
3. Nunnemann S, Wohlschläger AM, Ilg R, et al. Accelerated aging of the putamen in men but not in women. Neurobiol Aging 2009; 30:147–151.
4. Sato K, Taki Y, Fukuda H, Kawashima R. Neuroanatomical database of normal Japanese brains. Neural Netw 2003; 16:1301–1310.
5. Draganski B, Gaser C, Busch V, Schuierer G, Bogdahn U, May A. Neuroplasticity: changes in grey matter induced by training. Nature 2004; 427: 311–312.
6. Doran SJ, Charles-Edwards L, Reinsberg SA, Leach MO. A complete distortion correction for MR images: I. Gradient warp correction. Phys Med Biol 2005; 50:1343–1361.
7. Janke A, Zhao H, Cowin GJ, Galloway GJ, Doddrell DM. Use of spherical harmonic deconvolu-

tion methods to compensate for nonlinear gradient effects on MRI images. Magn Reson Med 2004; 52:115–122.
8. Jovicich J, Czanner S, Greve D, et al. Reliability in multi-site structural MRI studies: effects of gradient non-linearity correction on phantom and human data. Neuroimage 2006; 30:436–443.
9. Barnes J, Scahill RI, Boyes RG, et al. Differentiating AD from aging using semiautomated measurement of hippocampal atrophy rates. Neuroimage 2004; 23:574–581.
10. Thompson PM, Giedd JN, Woods RP, MacDonald D, Evans AC, Toga AW. Growth patterns in the developing brain detected by using continuum mechanical tensor maps. Nature 2000; 404: 190–193.
11. Gonoi W, Abe O, Yamasue H, et al. Age-related changes in regional brain volume evaluated by atlas-based method. Neuroradiology 2010; 52:865–873.
12. Leow AD, Klunder AD, Jack CR Jr., et al. Longitudinal stability of MRI for mapping brain change using tensor-based morphometry. Neuroimage 2006; 31:627–640.
13. Shuter B, Yeh IB, Graham S, Au C, Wang SC. Reproducibility of brain tissue volumes in longitudinal studies: effects of changes in signal-to-noise ratio and scanner software. Neuroimage 2008; 41: 371–379.
14. Han X, Jovicich J, Salat D, et al. Reliability of MRI-derived measurements of human cerebral cortical thickness: the effects of field strength, scanner upgrade and manufacturer. Neuroimage 2006; 32:180–194.
15. McRobbie DW, Quest RA. Effectiveness and relevance of MR acceptance testing: results of an 8 year audit. Br J Radiol 2002; 75:523–531.
16. Fazekas F, Chawluk JB, Alavi A, Hurtig HI, Zimmerman RA. MR signal abnormalities at 1.5T in Alzheimer's dementia and normal aging. AJR Am J Roentgenol 1987; 149:351–356.
17. Ashburner J, Friston KJ. Unified segmentation. Neuroimage 2005; 26:839–851.
18. Sled JG, Zijdenbos AP, Evans AC. A nonparametric method for automatic correction of intensity nonuniformity in MRI data. IEEE Trans Med Imaging 1998; 17:87–97.
19. Sumanaweera TS, Glover GH, Binford TO, Adler JR. MR susceptibility misregistration correction. IEEE Trans Med Imaging 1993; 12:251–259.
20. Sumanaweera TS, Glover GH, Hemler PF, et al. MR geometric distortion correction for improved frame-based stereotaxic target localization accuracy. Magn Reson Med 1995; 34:106–113.
21. Schad LR, Ehricke HH, Wowra B, et al. Correction of spatial distortion in magnetic resonance angiography for radiosurgical treatment planning of cerebral arteriovenous malformations. Magn Reson Imaging 1992; 10:609–621.
22. Chang TY, Hong JH, Yeh P. Spatial amplification: an image-processing technique using the selective amplification of spatial frequencies. Opt Lett 1990; 15:743–745.

Eur Radiol (2012) 22:1613–1623
DOI 10.1007/s00330-012-2452-z

COMPUTED TOMOGRAPHY

Model-based iterative reconstruction technique for radiation dose reduction in chest CT: comparison with the adaptive statistical iterative reconstruction technique

Masaki Katsura · Izuru Matsuda · Masaaki Akahane · Jiro Sato · Hiroyuki Akai · Koichiro Yasaka · Akira Kunimatsu · Kuni Ohtomo

Received: 22 December 2011 / Revised: 22 February 2012 / Accepted: 23 March 2012 / Published online: 27 April 2012

Abstract
Objectives To prospectively evaluate dose reduction and image quality characteristics of chest CT reconstructed with model-based iterative reconstruction (MBIR) compared with adaptive statistical iterative reconstruction (ASIR).
Methods One hundred patients underwent reference-dose and low-dose unenhanced chest CT with 64-row multidetector CT. Images were reconstructed with 50 % ASIR-filtered back projection blending (ASIR50) for reference-dose CT, and with ASIR50 and MBIR for low-dose CT. Two radiologists assessed the images in a blinded manner for subjective image noise, artefacts and diagnostic acceptability. Objective image noise was measured in the lung parenchyma. Data were analysed using the sign test and pair-wise Student's t-test.
Results Compared with reference-dose CT, there was a 79.0 % decrease in dose–length product with low-dose CT. Low-dose MBIR images had significantly lower objective image noise (16.93±3.00) than low-dose ASIR (49.24± 9.11, $P<0.01$) and reference-dose ASIR images (24.93± 4.65, $P<0.01$). Low-dose MBIR images were all diagnostically acceptable. Unique features of low-dose MBIR images included motion artefacts and pixellated blotchy appearances, which did not adversely affect diagnostic acceptability.
Conclusion Diagnostically acceptable chest CT images acquired with nearly 80 % less radiation can be obtained using MBIR. MBIR shows greater potential than ASIR for providing diagnostically acceptable low-dose CT images without severely compromising image quality.

M. Katsura (✉) · I. Matsuda · M. Akahane · J. Sato · H. Akai · K. Yasaka · A. Kunimatsu · K. Ohtomo
Department of Radiology, Graduate School of Medicine, The University of Tokyo,
7-3-1 Hongo,
Bunkyo-ku, Tokyo 113-8655, Japan
e-mail: mkatsura-tky@umin.ac.jp

Key Points
- *Model-based iterative reconstruction (MBIR) creates high-quality low-dose CT images.*
- *MBIR significantly improves image noise and artefacts over adaptive statistical iterative techniques.*
- *MBIR shows greater potential than ASIR for diagnostically acceptable low-dose CT.*
- *The prolonged processing time of MBIR may currently limit its routine use in clinical practice.*

Keywords Model-based iterative reconstruction · Adaptive statistical iterative reconstruction · Radiation dose reduction · Image noise · Spatial resolution

Abbreviations and acronyms

MBIR	Model-based iterative reconstruction
ASIR	Adaptive statistical iterative reconstruction
FBP	Filtered back projection
MTF	Modulation transfer function
ED	Effective dose

Introduction

There are increasing concerns about the magnitude of the radiation dose delivered in computed tomography (CT) and the potential increase in the incidence of radiation-induced carcinogenesis [1]. The estimated annual effective dose (ED) from medical radiation exposure per individual in the United States (US) population has increased about six-fold over the past quarter century (from 0.53 mSv in 1980 to 3.0 mSv in 2006) [2]. This dramatic increase is largely attributable to the rapid

and substantial rise in CT utilisation (from 3,000,000 studies in the US in 1980 to 70,000,000 studies in 2006) [3]. Despite several activities that have been conducted to monitor and reduce the radiation dose delivered to patients [3], the US per capita ED from CT examinations in 2006 increased to 1.47 mSv, amounting to almost one half of total medical exposure [4].

Several dose-reduction techniques, such as tube current modulation [5], reduced tube voltage [6], use of a higher pitch [7] and noise reduction filters [8], have been successfully implemented and have been shown to reduce radiation exposure. However, further reductions in radiation dose are hindered by increased image noise and degraded image quality, mainly as a result of limitations of the standard filtered back projection (FBP) reconstruction algorithm currently used on most CT systems. Use of an iterative reconstruction (IR) algorithm is an alternative image reconstruction technique. Unlike conventional FBP, which is based on simpler mathematical assumptions of the tomographic imaging system, IR generates a set of synthesised projections by accurately modelling the data collection process in CT. One of the first IR algorithms released for clinical use was the adaptive statistical iterative reconstruction (ASIR) algorithm (GE Healthcare, Waukasha, WI, USA). Previous phantom and clinical studies have shown that ASIR provides diagnostically acceptable images with a reduction in image noise for low-radiation dose CT compared with the FBP algorithm [9–18].

The recently developed model-based iterative reconstruction (MBIR) is a much more complex and advanced IR technique than ASIR [19, 20] (see Appendix 1). Phantom experiments have shown that MBIR provides a significant reduction in image noise and streak artefacts, a significant improvement in spatial resolution, and has the potential to allow further radiation dose reduction without compromising image quality [19]. However, few data are available on its effect on radiation dose reduction in patients, and there are no clinical studies to our knowledge that have directly compared MBIR with ASIR. The purpose of this study was to evaluate dose reduction and image quality characteristics of three different chest CT protocols in the same patients: low-dose CT reconstructed with MBIR, low-dose CT reconstructed with ASIR and reference-dose CT reconstructed with ASIR.

Materials and methods

This prospective clinical study was compliant with Health Insurance Portability and Accountability Act guidelines and was approved by the Human Research Committee of our Institutional Review Board.

Patients

The Radiology Information System was checked to identify patients scheduled for unenhanced standard-of-care clinical chest CT examinations (around 5–10 per day) at a single tertiary care centre. Inclusion criteria for the present study were the following: age ≥18 years, the patient was scheduled for unenhanced standard-of-care CT examination of the chest, the ability to give written informed consent, and the ability to hold one's breath and remain still for at least 10 s. Patients who were unable to provide written informed consent, follow verbal commands for breath holding or remain still for the duration of CT acquisition were excluded. Women who were pregnant or were trying to get pregnant were also excluded.

Each potential subject was given a detailed informed consent form written in simple language about the objective, method and risks of study participation. The study procedure, which involved an acquisition of reference-dose CT followed by low-dose CT (both discussed later in detail), was explained to the subjects. They were also informed that the sum of reference-dose and low-dose CT acquisition would not exceed the radiation dose for standard-of-care chest CT at our institution. The risks associated with study participation, particularly the possible influence on diagnostic performance, in which the reference dose in the present study was expected to be slightly lower compared to radiation doses for standard-of-care CT, were explained to the subjects in simple language. Subjects were also informed that they would not receive any remuneration or benefit from their participation in the study.

Between 1 July 2011 and 28 July 2011, 113 consecutive eligible patients were identified. Nine patients refused to participate in the study, and 104 gave informed consent to participation in the study. None withdrew from the study after signing the consent form. To understand the evaluation system, two thoracic radiologists (HA and IM, with 8 and 6 years of experience, respectively) were trained in the subjective grading of image quality using the images of 4 patients, who were selected from the 104 patients using a random number table, and subsequently eliminated from the rest of the analysis. Therefore, 100 patients were included in the final analysis. The body weight of each patient was recorded as well as other demographic information (summarised in Table 1).

CT data acquisition

Unenhanced chest CT for reference-dose CT followed by low-dose CT (discussed later) were acquired with a 64-row multidetector CT system (Discovery CT750 HD; GE Healthcare). All patients in the study were able to undergo chest CT in the supine position with both arms elevated and with a single breath-hold for each acquisition. In this

Table 1 Patient characteristics and CT parameters

Men/women	55/45
Age (years)	65.6±12.4
Body weight (kg)	58.0±13.0
Acquisition mode	Helical
Tube voltage (kVp)	120
Field of view (mm)	350*
Gantry rotation time (s)	0.5
Table speed (mm per gantry rotation)	39.37
Detector configuration (mm)	64×0.625
Reconstructed section thickness (mm)	0.625
Pitch	0.984:1

Data are mean±standard deviation for each value unless indicated otherwise. A field of view of 350 mm was typically set; however, it was adjusted according to patient size (*). The main clinical indications for chest CT were as follows: follow-up for a pulmonary nodule (n=23), abnormal chest radiograph (n=19), interstitial lung disease (n=17), staging or restaging of known or suspected malignancy (n=13), ground-glass opacity (n=7), nontuberculous mycobacterial disease (n=6), obstructive pulmonary disease (n=4), haemoptysis (n=3), pulmonary tuberculosis (n=2), sarcoidosis (n=2), mediastinal mass (n=2), hypersensitivity pneumonitis (n=1) and asbestosis (n=1)

prospective clinical study, reference- and low-dose CTs were acquired with minimal differences in data acquisition conditions (with the exception of radiation dose). For instance, to minimise the positional difference between the two acquisitions for each patient, the time between completion of the reference-dose CT and initiation of imaging for low-dose CT was kept to a minimum (about 10 s or less). To avoid contrast enhancement bias owing to the delay in imaging from the start of the injection, only unenhanced CT images were included in this study. Imaging parameters for both acquisitions were held constant with the exception of noise index (NI, discussed later) and are summarised in Table 1. For reconstructing both reference-dose and low-dose CT images, we used the chest kernel (a proprietary kernel of GE Healthcare), which is equivalent to the lung kernel for depiction of lung and equivalent to the soft-tissue kernel for depiction of mediastinal soft-tissue structures [21, 22].

Rationale for slice thickness

All images were reconstructed with axial slices 0.625 mm thick, which is standard in our institution for reading high-resolution CT of the chest. Images with increased slice thickness or coronal/sagittal reformats were not used for evaluation in this study for the following reasons. It is known that image noise is dependent on the reconstruction thickness, as thicker slice reconstructions are less noisy than thinner slice reconstructions. Generally, image noise is inversely proportional to the square root of the slice thickness (e.g. by increasing slice thickness from 0.625 mm to 2.5 mm=4×0.625, image noise should decrease by a factor of 1 divided by the square root of 4). However, our preliminary results of phantom experiments indicate that this does not necessarily apply to MBIR, and the relationship between image noise and slice thickness is different depending on the reconstruction algorithm (unpublished data). Furthermore, MBIR and ASIR behave differently in terms of image noise when reformatted into coronal and sagittal slices (also unpublished data). Therefore, to directly compare image quality characteristics, only 0.625-mm-thick axial slices were used in the present study.

Noise index setting

Both reference- and low-dose CT protocols involved the use of automatic tube current modulation (ATCM; Auto mA 3D; GE Healthcare). The operator-selected NI level modulates the tube current during gantry rotation to achieve a predicted average statistical noise level in the images of the specified reconstruction slice thickness requested. In this study, a fixed NI of 31.5 was used for reference-dose CT and of 70.44 was used for low-dose CT. Both NIs are the predicted noise level at a slice thickness of 0.625 mm. The rationale for the NI setting in the present study is described in Appendix 2.

Image reconstruction

Images for reference-dose CT were reconstructed with blending of 50 % filtered back projection and 50 % ASIR image data (ASIR50). A blending factor of 50 % was chosen based on the previous literature [16, 17] and recommendations from the vendor. Images for low-dose CT were reconstructed with ASIR50 and MBIR. Blending with FBP does not apply to MBIR, as it is a pure IR technique (see Appendix 1). Thus, three image data sets (reference-dose ASIR, low-dose ASIR and low-dose MBIR) were generated in each patient (Fig. 1). Each image data set was coded, patient information was removed and the data sets were randomised before blinded evaluation (Fig. 2).

Objective image quality

Objective measurements were performed for the image data sets of 100 patients (300 image sets) on a workstation (Centricity RA1000; GE Yokogawa Medical Systems) by a radiologist (MK) with 4 years of imaging experience. Circular regions of interest (ROI) were drawn in the descending thoracic aorta at the level of the carina (15–20 mm in diameter) for each image data set. Calcifications, soft plaques of the aortic wall and areas with prominent streak artefacts were carefully avoided. Circular ROIs were also drawn in the homogeneous part of the lung parenchyma at the level of the

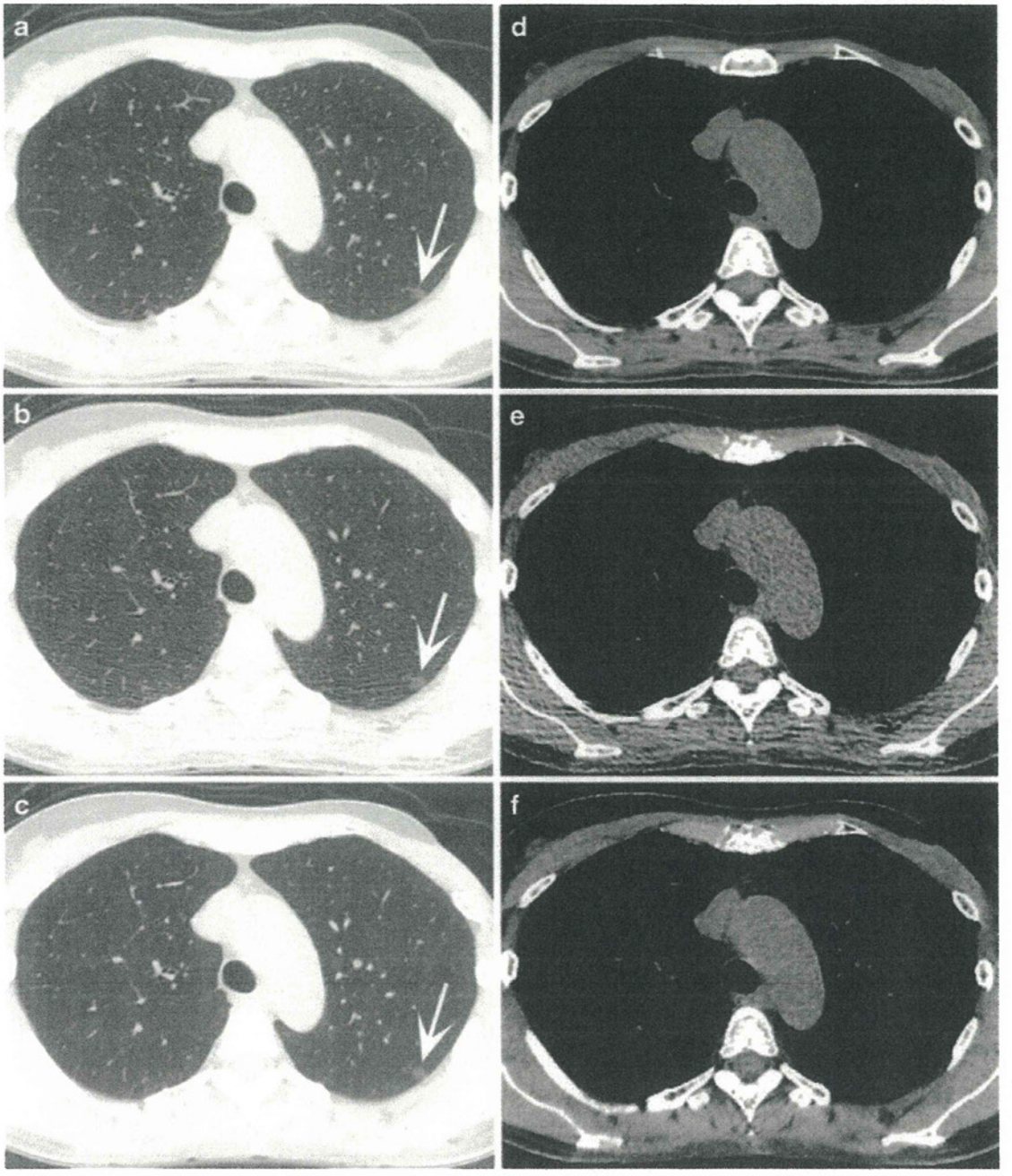

Fig. 1 (a, d) Reference-dose CT images [dose–length product (DLP), 191.10 mGy/cm] reconstructed with adaptive statistical iterative reconstruction (ASIR), (b, e) low-dose CT images (DLP, 38.45 mGy/cm) reconstructed with ASIR and (c, f) low-dose CT images reconstructed with model-based iterative reconstruction (MBIR) in a 58-year-old woman (weight, 50 kg). The prominent streak artefact from the shoulders on low-dose ASIR images (b, e) interferes with adequate visualisation of the ground-glass opacity nodule in the left upper lobe (b, arrow), which renders the image "unacceptable for diagnostic interpretation". Significant improvements in image noise and streak artefacts are observed in low-dose MBIR (c, f), and the nodule is clearly depicted (c, arrow). Low-dose MBIR CT images in this patient have equivalent image quality to reference-dose ASIR CT images (a, d) and were graded as "fully diagnostically acceptable" by both readers. Images are shown in lung [a–c; window width (WW), 1,500 HU; window length (WL), -600 HU] and mediastinal (d–f; WW, 400 HU; WL, 40 HU) window settings

carina (approximately 10 mm in diameter). The mean and standard deviation (i.e. objective image noise) of the CT values (HU) within the ROI were recorded. To evaluate the radiation dose, the estimated CT dose index volume (CTDIvol) and dose–length product (DLP) were recorded for each image data set following completion of the CT examination, according to the dose report. EDs were estimated from DLP using a constant of

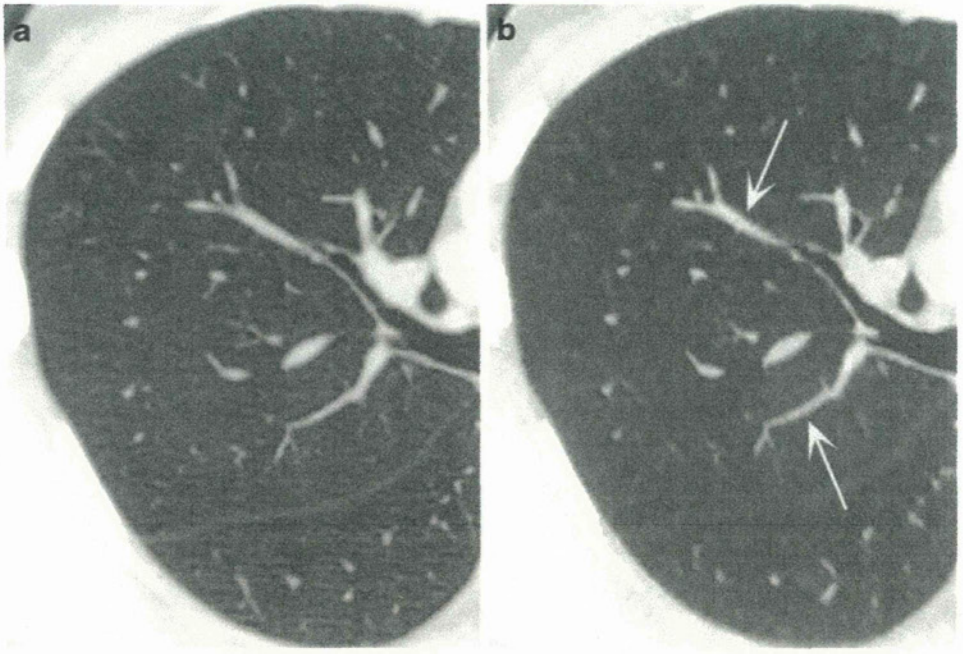

Fig. 2 Reference-dose ASIR (a; CTDIvol, 4.22 mGy; and DLP, 150.43 mGy/cm) and low-dose MBIR (b; CTDIvol, 0.85 mGy; and DLP, 30.24 mGy/cm) chest CT images obtained in a 53-year-old woman weighing 46 kg are shown in the lung (WW, 1,500 HU; WL, -600 HU) window setting. Note the blotchy, pixellated appearance (arrows) in b compared with a

0.014 mSv/mGy-cm as described in the report of the national survey conducted in the UK in 2003 (NRPB W67) [25]. Radiation dose descriptors in the present study were compared with the typical dose described in the NRPB W67 report [25].

Subjective image quality

Two thoracic radiologists (HA and IM) independently assessed the image data sets of 100 patients (300 image sets) for image quality using a commercial software package (EV Insite, PSP Corp., Tokyo, Japan). At the time of the present study, both radiologists already had 2.5 years of experience with ASIR images, which were introduced to our department in January 2009. They had little experience with MBIR images at the time of the present study, although they became familiar with them in the training session. In addition to the default preselected lung window settings [window width (WW), 1,500 Hounsfield units (HU), window level (WL), -600 HU] and mediastinal window settings (WW, 400 HU; WL, 40 HU), radiologists were allowed to change the WW and WL for ease of assessment. Both radiologists were blinded to patient data, clinical information and image reconstruction techniques.

For each image data set, each radiologist graded subjective image noise, artefacts, critical reproduction of visually sharp chest structures and diagnostic acceptability (see Appendix 3 for details). Image quality characteristics assessed in this study have been described in the European Guidelines on Quality Criteria for Computerised Tomography [26] and have been used in multiple previous studies in the radiology literature [13, 14, 16, 17]. To assess intraobserver agreement, 10 patients (30 image sets) were randomly selected from the 100 patients and these 30 images sets were analysed twice. Consequently, 330 image sets were analysed in a blinded and randomised manner by each radiologist.

Estimation of modulation transfer function

To compare the effect of MBIR, ASIR and FBP reconstructions on spatial resolution, we performed a phantom study to estimate the modulation transfer function (MTF) by using the same system used for imaging patients as that described above. A phantom (Catphan 600; The Phantom Laboratory, Salem, NY, USA) with a 28-mm-diameter tungsten wire was imaged at a tube current of 120 kVp, with 200 mA, a helical acquisition mode, a section thickness of 0.625 mm, a 0.5-s gantry rotation time and a standard reconstruction kernel (a proprietary kernel of GE Healthcare). Images were reconstructed with the MBIR technique, with 50 % and 100 % ASIR techniques, and with the FBP technique. The MTF was measured at the iso-centre and 10 cm off centre as the angular average of the two-dimensional Fourier transform of the point spread function in each of the reconstructed image data sets.

Statistical analysis

The data were analysed using JMP 9.0.0 software (SAS Institute, Cary, NC, USA). Whenever possible, results were expressed as the mean±the standard deviation. Inter- and intraobserver agreement for the two radiologists was estimated for the subjective image quality parameters using

Cohen's weighted kappa (κ) analysis. The following κ values were used to indicate agreement: 0.00–0.20, poor agreement; 0.21–0.40, fair agreement; 0.41–0.60, moderate agreement; 0.61–0.80, good agreement; and 0.81–1.00, excellent agreement. A sign test was used for each reader to compare subjective image quality assessments between image pairs. A Student's paired t-test was used to determine the significance of differences in objective image noise between image pairs. To reduce the possibility of significance due to chance because of multiple statistical testing, a Bonferroni correction was applied to the P value and significance was assumed only when the P value was <0.016.

Results

Radiation dose

Radiation dose descriptors for chest CT examinations acquired with reference-dose and low-dose CT for all 100 patients are summarised in Table 2. Compared with reference-dose CT, there was a 79.1 % decrease in CTDIvol and a 79.0 % decrease in DLP with low-dose CT. For direct comparison of the radiation dose with NRPB W67 [25], Table 3 selects out patients weighing 65–75 kg (11 patients; 9 male; age, 71.9±7.9 years; body weight, 67.6±2.2 kg). For these patients, the DLP and ED for reference-dose CT (395.5 mGy/cm, 5.54 mSv) were equivalent to the typical dose described in NRPB W67 for chest CT examinations of adults with a mean weight of about 70 kg (400 mGy/cm, 5.6 mSv) [25]. The ED for low-dose CT (1.13 mSv) was equivalent to the average ED for low-dose CT described in the NLST (1.5 mSv) [24].

Objective image quality

Low-dose MBIR images had significantly lower quantitative image noise in the lung parenchyma (16.93±3.00) than low-dose ASIR images (49.24±9.11, P<0.01) and reference-dose ASIR images (24.93±4.65, P<0.01, Table 4).

Table 2 Comparison of the radiation dose for reference- and low-dose CT

	Reference-dose	Low-dose
CTDIvol (mGy)	7.83±2.14	1.63±1.09
DLP (mGy/cm)	288.8±162.8	60.7±43.5
ED (mSv)	4.04	0.85

Data are mean±standard deviation for each value. CTDIvol=CT dose index volume, DLP=dose–length products, ED=effective dose for chest CT determined using a constant of 0.014 mSv/mGy/cm. Compared with reference-dose CT, there was a 79.1 % decrease in CTDIvol and a 79.0 % decrease in DLP with low-dose CT

Table 3 Radiation dose in patients weighing from 65 to 75 kg

	Reference-dose	Low-dose
CTDIvol (mGy)	10.83±2.92	2.20±0.65
DLP (mGy/cm)	395.5±106.3	80.7±24.5
ED (mSv)	5.54	1.13

Data are mean±standard deviation of each value. CTDIvol=CT dose index volume, DLP=dose–length products, ED=effective dose for chest CT determined using a constant of 0.014 mSv/mGy/cm. For 11 patients weighing from 65 kg to 75 kg (9 male and 2 female, age 71.9±7.9 years, body weight 67.6±2.2 kg), DLP and ED for reference-dose CT were equivalent to the typical dose described in NRPB W67 for chest CT examinations of adults with a mean weight of about 70 kg (400 mGy/cm, 5.6 mSv) [25]. The ED for low-dose CT was equivalent to the average ED for low-dose CT described in the NLST (1.5 mSv) [24]

Conversely, objective image noise in the descending aorta with MBIR (12.76±1.25) was significantly lower than with low-dose ASIR (23.42±3.83, P<0.01), but was significantly higher than with reference-dose ASIR (10.01±1.35, P< 0.01). Mean CT values within the ROI placed in the lung parenchyma or the descending aorta did not differ significantly (P>0.10 for each) among reference-dose ASIR, low-dose ASIR and low-dose MBIR.

Subjective image quality

Interobserver agreement between the two radiologists was excellent (κ=0.81–0.96) for subjective image noise, pixellated blotchy appearance and diagnostic acceptability, whereas it was moderate (κ=0.41–0.52) for motion and streak artefacts. Intraobserver agreement for each reader

Table 4 Objective image quality (mean CT value and image noise) measured within each region of interest

Region of interest	Reference-dose ASIR	Low-dose ASIR	Low-dose MBIR
Lung parenchyma (CT value)	-891.73±27.66	-889.78±28.68	-889.18±28.25
Lung parenchyma (image noise)	24.93±4.65*	49.24±9.11*	16.93±3.00*
Descending aorta (CT value)	38.05±5.21	37.26±7.28	36.86±5.76
Descending aorta (image noise)	10.01±1.35†	23.42±3.83†	12.76±1.25†

Data are mean±standard deviation (in HU). Image noise was expressed as the standard deviation of the CT values within the region of interest. Image noise was significantly lower (*P<0.01, Student's paired t-test) in low-dose MBIR than in reference-dose ASIR images for the lung parenchyma; however, it was significantly higher (†P<0.01) for the descending aorta. Mean CT values location did not differ significantly irrespective of region of interest (P>0.10 for all) among reference-dose ASIR, low-dose ASIR and low-dose MBIR images.

was excellent for subjective image noise, pixellated blotchy appearance and diagnostic acceptability (κ=0.80–1.00). Intraobserver agreement was variable for motion artefacts (κ=0.35 for reader 1 and κ=0.51 for reader 2) and streak artefacts (κ=0.96 for reader 1 and κ=0.67 for reader 2).

Subjective image noise, image artefacts and diagnostic acceptability with MBIR and ASIR techniques are summarised in Table 5 (also see Appendix 3 for details of subjective scores). For subjective image noise, modal scores were "less than average" for low-dose MBIR and "average" for reference-dose ASIR ($P<0.001$ for both readers). None of the low-dose MBIR images was graded with "substantial" or "unacceptable image noise". Conversely, low-dose ASIR images were typically associated with "substantial" or "unacceptable image noise" ($P<0.001$ each vs. the other two image data sets for both readers). For diagnostic acceptability, modal scores were "fully acceptable" or "probably acceptable" for low-dose MBIR and "fully acceptable" for reference-dose ASIR ($P<0.001$ for reader 2). There were no "diagnostically unacceptable" low-dose MBIR images, whereas low-dose ASIR images were typically graded as "diagnostically unacceptable" ($P<0.001$ each vs. the other two image data sets for both readers).

While streak artefacts were unapparent or minimally recognisable in most reference-dose ASIR images, streak artefacts not affecting diagnostic interpretation were noted in some low-dose MBIR images, with variability between readers ($P>0.90$ for reader 1 and $P=0.0023$ for reader 2). Low-dose MBIR images were also more often associated with motion artefacts and pixellated blotchy appearance compared with ASIR images ($P<0.001$ for both readers). However, neither of the artefacts affected diagnostic interpretation.

Pixellated blotchy appearance resulted in a step-like appearance at the tissue interfaces and notably affected the sharp visualisation of the following anatomical structures in low-dose MBIR images: pulmonary fissures (13/100 for reader 1, 18/100 for reader 2; $P<0.001$ each vs. reference- and low-dose ASIR for reader 2), the small peripheral lung vessel walls and bronchus (8/100 for reader 1, 1/100 for reader 2; $P<0.001$ each vs. reference- and low-dose ASIR for reader 1) and the border between the pleura and the thoracic wall (84/100 for reader 1, 7/100 for reader 2; $P<0.001$ each vs. reference- and low-dose ASIR for both readers).

MTF estimation

Results of the estimation of the MTF, or spatial resolution, are summarised in Fig. 3. There was consistent improvement both at the iso-centre and off centre in the spatial resolution of images reconstructed with MBIR compared with the ASIR and the FBP images at 5 %, 10 % and 50 % MTF.

Discussion

In this prospective study of 100 patients, image quality characteristics of low-dose chest CT reconstructed with MBIR and ASIR, and reference-dose chest CT reconstructed with ASIR were compared. In chest CT images acquired with nearly 80 % less radiation (low-dose CT), significant improvements in image noise and streak artefacts were observed with the use of MBIR compared with ASIR. Low-dose CT images obtained using MBIR were diagnostically acceptable. To the best of our knowledge, this is the first prospective clinical study to evaluate CT radiation dose reduction in the same patients and compare image quality characteristics with two different reconstruction methods, MBIR and ASIR.

For low-dose CT, MBIR significantly improved objective image noise in the lung parenchyma compared with ASIR.

Table 5 Subjective image quality scores for the two radiologists (reader 1 and reader 2)

Image quality	Reader 1			Reader 2		
	Reference-dose ASIR	Low-dose ASIR	Low-dose MBIR	Reference-dose ASIR	Low-dose ASIR	Low-dose MBIR
Noise (1/2/3/4/5)	0/0/99/1/0*	0/1/5/59/5*	0/100/0/0/0*	0/1/98/1/0*	0/1/8/61/30*	8/75/17/0/0*
Motion artefact (1/2/3)	96/4/0‡	95/5/0‡	77/23/0‡	94/6/0‡	95/4/1‡	58/38/4‡
Streak artefact (1/2/3)	99/1/0†	6/12/82†	98/2/0†	97/2/1**	27/67/6**	83/16/1**
Pixellated blotchy appearance (1/2/3)	100/0/0‡‡	99/1/0‡‡	1/99/0‡‡	100/0/0‡‡	99/1/0‡‡	4/96/0‡‡
Diagnostic acceptability (1/2/3/4)	99/1/0/0††	6/10/49/35††	94/6/0/0††	97/2/1/0 ***	8/13/49/30***	41/53/6/0***

Data show the frequency of numerical scores given in each category for the 100 patients. Using a sign test, the subjective score differences were statistically significant between all pairs in image noise for both readers (*$P<0.001$), in streak artefacts for reader 2 (**$P<0.003$) and in diagnostic acceptability for reader 2 (***$P<0.001$). The subjective score differences of low-dose ASIR vs. reference-dose ASIR, and low-dose ASIR vs. low-dose MBIR were significant with regard to streak artefacts for reader 1 (†$P<0.001$) and in diagnostic acceptability for reader 1 (††$P<0.001$). The subjective score differences of low-dose MBIR vs. reference-dose ASIR, and low-dose MBIR vs. low-dose ASIR were significant with regard to motion artefacts for both readers (‡$P<0.001$), and in pixellated blotchy appearance for both readers (‡‡$P<0.001$)

Compared with reference-dose ASIR, objective image noise in the lung parenchyma was significantly lower with low-dose MBIR than with reference-dose ASIR; however, the results were the opposite in the descending aorta. This may be for the following reason: it is acknowledged that reconstruction kernels used for FBP images can largely influence objective image noise in FBP and subsequently in ASIR-FBP-blended images (50 %/50 % blending was used in the present study). High-pass filter algorithms preserve the higher spatial frequencies at the expense of greater noise, whereas low-pass filter algorithms reduce the higher frequency contribution, which decreases noise but also degrades spatial resolution. The chest kernel used in the present study is equivalent to a high-pass filter algorithm (e.g. the lung kernel) for depiction of the lung and is equivalent to a low-pass filter algorithm (e.g. the soft-tissue kernel) for depiction of the mediastinal soft tissue [21, 22]. Therefore, the mixed results between the lung parenchyma and the aorta for objective image noise can be largely explained by the reconstruction kernel.

Image features uniquely noted in the MBIR-reconstructed images in the present study included motion artefacts and a pixellated blotchy appearance. The reason why there are greater motion artefacts with MBIR than with ASIR images is not clear; however, it may be due to differences in time resolution between MBIR and ASIR, and needs to be fully investigated in future studies. The exact reasons for the pixellated blotchy appearance uniquely seen on MBIR are also unknown; inherent differences in image reconstruction may have contributed to these differences. One can argue that the pixellated blotchy appearance may be ascribed to lower spatial resolution; however, our phantom study shows consistent improvement in the spatial resolution of images reconstructed with MBIR compared with the ASIR (Fig. 3). A pixellated blotchy appearance has been described in many initial ASIR reports [9, 14–17]. However, this appearance was not prominently seen on ASIR images in the present study, which, according to the vendor, can be attributed to the advancements of the ASIR algorithm that have been made following the earlier studies. A pixellated blotchy appearance on MBIR images resulted in a step-like appearance at the tissue interfaces and affected the sharp visualistion of some anatomical structures (rated "not sharply visualised"), such as the pulmonary fissures, small pulmonary vessels and bronchi, and the border between the pleura and the thoracic wall. Overall, these MBIR-unique image features were not overly distracting in the present study and had little effect on diagnostic acceptability. However, the difference in image appearance and lack of reader familiarity may have contributed to the variability between the readers, particularly in the subjective evaluation of some image artefacts and anatomical structures. This variability should decrease over the course of familiarisation with MBIR images and may decrease even more if the MBIR-unique image appearance becomes less prominent with further advancement of the MBIR algorithm.

The radiation dose delivered by low-dose CT in the present study was almost equivalent to the dose described in NLST [24]. As the present results indicate that MBIR has a greater potential than ASIR to provide diagnostically acceptable low-dose CT images without severely compromising image quality, MBIR is expected to be helpful particularly in certain patients and settings, such as imaging infants and young patients or screening for lung cancer. The ability of MBIR to detect and localise lesions not only in the chest but also in different body regions needs to be investigated in further clinical studies. Although not assessed in the present study, the behaviour of MBIR concerning image noise at increased slice thicknesses (e.g. 2.5–5 mm) and in coronal/sagittal reformats, which may be used by many radiologists for clinical work, needs to be further investigated in clinical studies. The influence of other dose-reduction techniques such as reducing tube voltage on MBIR should also be assessed in future studies. Another issue to consider for MBIR in a practical setting is the long reconstruction time. Although recent advances have reduced this time to about 1 h per case (the reconstruction time in the present report was not recorded as it was not a feature in the application software), MBIR may not yet be suitable for evaluation in acute clinical settings.

Several limitations of this study must be considered. First, all of the chest CT examinations were performed without intravenous contrast medium administration. The presence of streak artefacts from the superior vena cava is one important issue that needs to be considered in contrast-enhanced chest CT images, and the performance of MBIR with regard to these streaks should be fully investigated in future studies. Second, although MBIR is expected to be helpful in low-dose CT for paediatric patients, patients under the age of 18 were not included in the study. Third, the body size of the patients in this study was generally small. MBIR has not yet been assessed in extremely large or obese patients, and this needs to be investigated in future studies. A fourth limitation of the study is that the results may not apply to other similar iterative reconstruction methods available from other vendors; fifth, owing to the difference in image appearance, blinding of the radiologists between MBIR and ASIR during subjective image analysis was difficult. However, we randomised the image sets acquired with different dose levels and reconstruction techniques.

In conclusion, chest CT images acceptable for diagnostic interpretation acquired with nearly 80 % less radiation can be obtained with the use of MBIR. MBIR

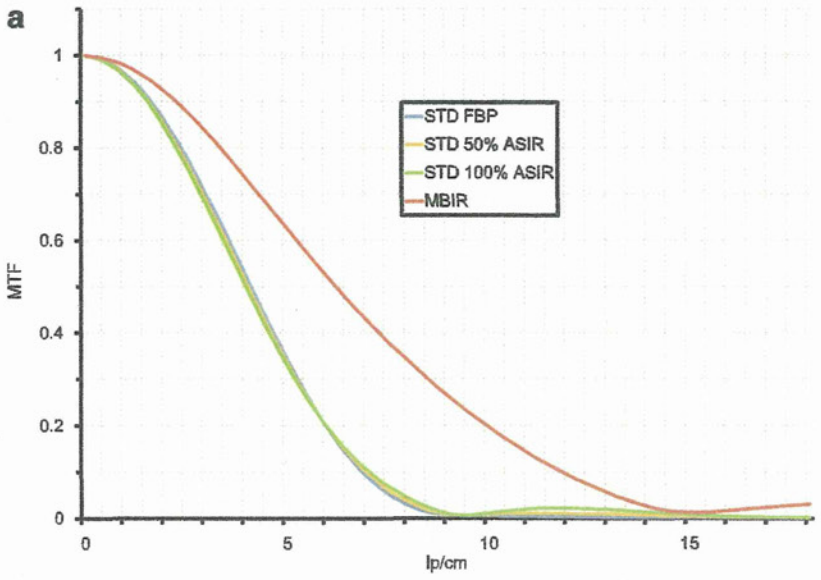

	STD FBP	STD 50% ASIR	STD 100% ASIR	MBIR
50% MTF (lp/cm)	4.12	4.05	3.99	6.40
10% MTF (lp/cm)	6.86	6.94	7.04	11.81
5% MTF (lp/cm)	7.54	7.68	7.86	13.04

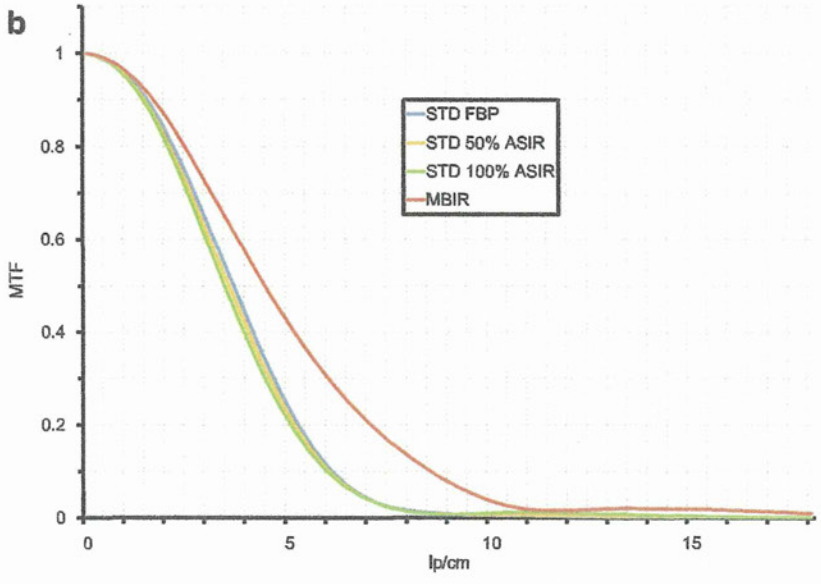

	STD FBP	STD 50% ASIR	STD 100% ASIR	MBIR
50% MTF (lp/cm)	3.62	3.52	3.41	4.41
10% MTF (lp/cm)	6.07	6.00	5.93	8.50
5% MTF (lp/cm)	6.76	6.72	6.69	9.58

Fig. 3 Line graph summarises modulation transfer function (MTF) at the iso-centre (a) and at 10 cm off centre (b) for 0.625-mm images CT reconstructed with filtered back projection (FBP), ASIR (50 % and 100 %) and MBIR. Compared with the ASIR and FBP images, MBIR images had higher spatial resolution at 5 %, 10 % and 50 % MTF. lp/cm=Line pairs per centimetre, STD=standard kernel

shows greater potential than ASIR for providing diagnostically acceptable low-dose CT images without severely compromising image quality. MBIR is expected to be helpful for dose reduction, particularly in certain patients and settings, such as imaging of infants and young patients and screening for lung cancer.

Acknowledgements We gratefully acknowledge Kosuke Sasaki, M.S., and Koji Segawa, R.T., for their technical support and assistance in data acquisition.

Appendix 1

ASIR and MBIR are new iterative reconstruction (IR) algorithms. Unlike the conventional FBP, which is based on simpler mathematical assumptions of the tomographic imaging system, IR generates a set of synthesised projections by accurately modelling the data collection process in CT. The model incorporates statistical system information (including photon statistics and electronic noise in the data acquisition system) and details of the system optics (including the size of each detector cell, dimensions of the focal spot, and the shape and size of each image voxel). The synthesised image is mathematically compared and corrected with the actual measurement in order to adjust estimation of the object's image. The technique then iterates this comparison and correction step in order to achieve close proximity between actual and measured projections. Inconsistencies in the projection measurement due to limited photon statistics and electronic noise are corrected with multiple iterations. These data-processing steps help to improve image quality from the noise and resolution perspectives, but prolong the reconstruction duration compared with FBP because of the intensive computations particularly required for incorporating system optics information.

The ASIR technique models just the photons and electronic noise statistics that primarily affect image noise, which are not as computationally intensive or time-consuming. This enables near real-time display of images at the time of imaging. ASIR also differs from other IR techniques in that the vendor provides a blending tool to blend the FBP with the ASIR images. This is accomplished by reconstruction of CT raw data with both FBP and ASIR techniques and then performing a weighted summation of each data set for the final reconstructed images. Prior phantom and clinical studies have already shown that ASIR provides diagnostically acceptable images with a reduction in image noise for low-radiation dose CT compared with the FBP algorithm [9–18].

The MBIR technique, on the other hand, is a pure IR technique that does not involve blending with FBP images, and is mathematically more complex and accurate than ASIR. MBIR not only incorporates modelling of photon and noise statistics like ASIR, it also involves modelling of system optics. This is unlike ASIR, which uses an idealised set of system optics (as does FBP), resulting in similar data utilisation per image. MBIR analyses the x-ray beam at the focal spot, then as it passes through the patient's body and again as it strikes the detector. The algorithm weights each data point so that noisy projections have less influence on the final results, and this allows more accurate image reconstruction. Phantom experiments have shown that MBIR has the potential to further reduce image noise, improve spatial resolution and thereby allow further dose reduction without compromising image quality [19]. With incorporation of system optics information and therefore a more accurate account of voxel and focal spot size and geometry, one can expect improvements in spatial resolution [19, 20]. Because MBIR is a complicated algorithm, using multiple iterations and multiple models, the reconstruction time is significantly longer than FBP as well as the other IR techniques, even with dedicated state-of-the-art parallel processors. The reconstruction time in the present study was about 1 h per case, although the exact time was not recorded as it was not a feature of the application software.

Appendix 2

The rationale for the NI setting in the present study is as follows. As the specified slice thickness for a given NI setting decreases by a factor of x, maintenance of the same radiation dose requires an increase in NI by a factor of 1 divided by the square root of x. According to the previous radiology literature [13, 23], the NI of 15.75 at a slice thickness of 2.5 mm has been used for reference-dose chest CT. Multiplying 15.75 by the square root of 4 (= 2.5/0.625) results in 31.5. Theoretically, the fixed NI of 31.5 at 0.625 mm should achieve the same radiation dose for reference-dose chest CT from the previous radiology literature. As for the NI setting for low-dose CT, we referred to the average ED for low-dose CT described in the National Lung Screening Trial (NLST, 1.5 mSv) [24], which is about one fifth of the radiation dose for reference-dose chest CT described in the previous radiology literature [13, 23]. As the radiation dose decreases by 1/y, the image noise increases by the square root of y. Multiplying the NI for reference-dose CT in the present study (= 31.5) by the square root of 5 results in an NI of 70.44.

Appendix 3

Subjective image noise was defined as overall graininess or mottle in the lung parenchyma, and was assessed in the lung window setting on a five-point scale (1=no or only minimal image noise, 2=less than average image noise, 3=average image noise, 4=more than average or substantial image noise that may interfere with diagnostic decision-making in less than half of the lung parenchyma, and 5=more than

average or substantial image noise that may interfere with diagnostic decision-making in more than half of the lung parenchyma). Artefacts were graded on a three-point scale (1=artefacts unapparent or only minimally recognisable, 2=artefacts recognised but not interfering with diagnostic decision-making, and 3=substantial artefacts recognised affecting diagnostic decision-making). The following artefacts were assessed: streak artefacts, motion artefacts due to heart wall motion and blotchy pixellated appearance at the tissue interface (Fig. 2b). Critical reproduction of visually sharp anatomical structures was assessed. The following anatomical structures were evaluated: pulmonary fissures; secondary pulmonary lobular structures such as interlobular arteries; large- and medium-sized pulmonary vessels; small pulmonary vessels; large- and medium-sized bronchi; small bronchi; the pleuromediastinal border; the border between the pleura and the thoracic wall; the thoracic aorta; anterior mediastinal structures including thymic residue; the trachea and main bronchi; paratracheal tissue; the carina and lymph node area; and the oesophagus. Diagnostic acceptability was assessed on a four-point scale (1=fully acceptable, 2=probably acceptable, 3=deemed acceptable only for limited clinical conditions, and 4=unacceptable).

References

1. Brenner DJ, Hall EJ (2007) Computed tomography—an increasing source of radiation exposure. N Engl J Med 357:2277–2284
2. Schauer DA, Linton OW (2009) NCRP report no. 160, ionizing radiation exposure of the population of the United States, medical exposure—are we doing less with more, and is there a role for health physicists? Health Phys 97:1–5
3. Amis ES Jr, Butler PF, Applegate KE et al (2007) American College of Radiology white paper on radiation dose in medicine. J Am Coll Radiol 4:272–284
4. Mettler FA Jr, Bhargavan M, Faulkner K et al (2009) Radiologic and nuclear medicine studies in the United States and worldwide: Frequency, radiation dose, and comparison with other radiation sources – 1950–2007. Radiology 253:520–531
5. Kalra MK, Maher MM, Toth TL et al (2004) Strategies for CT radiation dose optimization. Radiology 230:619–628
6. Heyer CM, Mohr PS, Lemburg SP, Peters SA, Nicolas V (2007) Image quality and radiation exposure at pulmonary CT angiography with 100- or 120-kVp protocol: Prospective randomized study. Radiology 245:577–583
7. Diel J, Perlmutter S, Venkataramanan N, Mueller R, Lane MJ, Katz DS (2000) Unenhanced helical CT using increased pitch for suspected renal colic: An effective technique for radiation dose reduction? J Comput Assist Tomogr 24:795–801
8. Kalra MK, Maher MM, Sahani DV et al (2003) Low-dose CT of the abdomen: Evaluation of image improvement with use of noise reduction filters pilot study. Radiology 228:251–256
9. Hara AK, Paden RG, Silva AC, Kujak JL, Lawder HJ, Pavlicek W (2009) Iterative reconstruction technique for reducing body radiation dose at CT: Feasibility study. AJR Am J Roentgenol 193:764–771
10. Flicek KT, Hara AK, Silva AC, Wu Q, Peter MB, Johnson CD (2010) Reducing the radiation dose for CT colonography using adaptive statistical iterative reconstruction: A pilot study. AJR Am J Roentgenol 195:126–131
11. Leipsic J, Labounty TM, Heilbron B et al (2010) Adaptive statistical iterative reconstruction: Assessment of image noise and image quality in coronary CT angiography. AJR Am J Roentgenol 195:649–654
12. Leipsic J, Nguyen G, Brown J, Sin D, Mayo JR (2010) A prospective evaluation of dose reduction and image quality in chest CT using adaptive statistical iterative reconstruction. AJR Am J Roentgenol 195:1095–1099
13. Prakash P, Kalra MK, Digumarthy SR et al (2010) Radiation dose reduction with chest computed tomography using adaptive statistical iterative reconstruction technique: Initial experience. J Comput Assist Tomogr 34:40–45
14. Prakash P, Kalra MK, Kambadakone AK et al (2010) Reducing abdominal CT radiation dose with adaptive statistical iterative reconstruction technique. Invest Radiol 45:202–210
15. Sagara Y, Hara AK, Pavlicek W, Silva AC, Paden RG, Wu Q (2010) Abdominal CT: Comparison of low-dose CT with adaptive statistical iterative reconstruction and routine-dose CT with filtered back projection in 53 patients. AJR Am J Roentgenol 195:713–719
16. Singh S, Kalra MK, Gilman MD et al (2011) Adaptive statistical iterative reconstruction technique for radiation dose reduction in chest CT: A pilot study. Radiology 259:565–573
17. Singh S, Kalra MK, Hsieh J et al (2010) Abdominal CT: Comparison of adaptive statistical iterative and filtered back projection reconstruction techniques. Radiology 257:373–383
18. Cornfeld D, Israel G, Detroy E, Bokhari J, Mojibian H (2011) Impact of adaptive statistical iterative reconstruction (ASIR) on radiation dose and image quality in aortic dissection studies: A qualitative and quantitative analysis. AJR Am J Roentgenol 196: W336–W340
19. Thibault JB, Sauer KD, Bouman CA, Hsieh J (2007) A three-dimensional statistical approach to improved image quality for multislice helical CT. Med Phys 34:4526–4544
20. Yu Z, Thibault JB, Bouman CA, Sauer KD, Hsieh J (2011) Fast model-based X-ray CT reconstruction using spatially nonhomogeneous ICD optimization. IEEE Trans Image Process 20:161–175
21. Strub WM, Weiss KL, Sun D (2007) Hybrid reconstruction kernel: Optimized chest CT. AJR Am J Roentgenol 189: W115–W116
22. Weiss KL, Cornelius RS, Greeley AL et al (2011) Hybrid convolution kernel: Optimized CT of the head, neck, and spine. AJR Am J Roentgenol 196:403–406
23. Prakash P, Kalra MK, Ackman JB et al (2010) Diffuse lung disease: CT of the chest with adaptive statistical iterative reconstruction technique. Radiology 256:261–269
24. National Lung Screening Trial Research Team, Aberle DR, Berg CD et al (2011) The National Lung Screening Trial: overview and study design. Radiology 258:243–253
25. Shrimpton PC, Hillier MC, Lewis MA, Dunn M (2006) National survey of doses from CT in the UK: 2003. Br J Radiol 79:968–980
26. EUR 16262. European guidelines on quality criteria for computed tomography. www.drs.dk/guidelines/ct/quality/. Accessed 10 February 2012

Jpn J Radiol (2012) 30:34–39
DOI 10.1007/s11604-011-0004-0

ORIGINAL ARTICLE

Precision of the measurement of CT numbers: comparison of dual-energy CT spectral imaging with fast kVp switching and conventional CT with phantoms

Izuru Matsuda · Masaaki Akahane · Jiro Sato · Masaki Katsura · Shigeru Kiryu · Naoki Yoshioka · Akira Kunimatsu · Kenji Ino · Kuni Ohtomo

Received: 27 May 2011 / Accepted: 21 July 2011 / Published online: 2 December 2011

Abstract
Purpose To compare dual-energy computed tomography (CT) spectral imaging and conventional CT imaging in terms of precision of the measurement of CT numbers in phantoms.
Materials and methods A circular phantom (CP) and an elliptical phantom (EP) were used. Capsules filled with iodine contrast media solutions at various concentration levels were placed in the phantoms. Conventional CT was performed at a tube voltage of 120 kVp. Simulated monochromatic images at 65 keV were obtained by dual-energy CT spectral imaging. The CT number of each iodine capsule was measured. A linear regression model was used to evaluate linearity, while analysis of covariance was used to investigate the degree of variability according to phantom shape for each imaging method.
Results With conventional imaging, the slopes of the regression lines for CT numbers measured at the EP center and EP periphery were significantly lower than those measured for CP ($P < 0.0001$ for both EP center vs. CP and for EP periphery vs. CP). No significant difference in slope was found among phantom shapes in dual-energy spectral CT imaging.
Conclusion Computed tomography numbers varied considerably depending on the phantom shape in conventional CT, whereas dual-energy CT provided consistent CT numbers regardless of the phantom shape.

Keywords Dual-energy CT · CT number · Precision · Phantom · Monochromatic imaging

I. Matsuda (✉) · M. Akahane · J. Sato · M. Katsura · A. Kunimatsu · K. Ohtomo
Department of Radiology, Graduate School of Medicine, The University of Tokyo, 7-3-1 Hongo, Bunkyo-ku, Tokyo 113-8655, Japan
e-mail: imatsuda-tky@umin.ac.jp

S. Kiryu
Department of Radiology, Institute of Medical Science, The University of Tokyo, 4-6-1 Shirokanedai, Minato-ku, Tokyo 108-8639, Japan

N. Yoshioka
Department of Integrated Imaging Informatics, The University of Tokyo Hospital, 7-3-1 Hongo, Bunkyo-ku, Tokyo 113-8655, Japan

K. Ino
Department of Clinical Radiology, The University of Tokyo Hospital, 7-3-1 Hongo, Bunkyo-ku, Tokyo 113-8655, Japan

Introduction

Computed tomography (CT) number is a calculated value and an estimate of the X-ray attenuation coefficient of a voxel, generally expressed in Hounsfield units (HU), where the CT number of air is −1000 HU and that of water is 0 HU. Despite its seemingly physical definition, values are reported to be variable, being dependent on factors such as the model of CT scanner, tube voltage, reconstruction algorithm, and distribution of the examined object [1–4]. A clinical example of the poor reproducibility of CT number has been reported as pseudoenhancement, such as increased attenuation of small simple renal cysts on contrast-enhanced CT scans [5–13].

Dual-energy CT methods are one of the most promising recent technological advances in CT. CT data acquisition is generally performed using a particular X-ray tube potential. By using two different X-ray spectra, dual-energy CT can distinguish pixels with the same CT number but that

consist of different materials, e.g., calcium, iodine, or uric acid [14–16]. In measuring the X-ray attenuation of an object using two different spectra, it is possible to resolve attenuation measurements in the density of two arbitrarily chosen materials. This mathematical process is termed 'material decomposition' [17]. Using this method, monochromatic images are synthesized from the material density images. The monochromatic image is the virtual image that would be obtained if the X-ray source produced only X-ray photons at a single energy. In general, the monochromatic image is similar to a conventional CT image, but has fewer artifacts, particularly beam-hardening artifacts [18].

One of the causes of the poor reproducibility of CT numbers is thought to be nonlinear errors due to scatter in attenuation measurement, which is difficult to correct adequately [19]. Also, it was reported that the material decomposition process in dual-energy CT imaging methods had a compensating effect for scatter [20]. The purpose of the present study is to compare dual-energy CT spectral imaging and conventional CT imaging in terms of the precision of measurements of CT numbers with phantoms.

Materials and methods

Phantoms

We used a 15-cm-diameter circular phantom (CP) and an elliptical phantom (EP), 22 cm in the anterior-posterior direction and 33 cm in the lateral direction, to evaluate the effect of the surrounding density distribution on CT number (Fig. 1). The CP was made of 15-cm-thick tough-water equivalent phantom (Kyoto Kagaku, Kyoto, Japan). Optimal CT number measurement with less error was represented by measurement in the CP. Five cylindrical holes of 1 cm diameter were placed circularly on the CP.

The EP (Multislice CT phantom MHT type; Kyoto Kagaku, Kyoto, Japan) was made of polyurethane with cylindrical holes located in the center and at the 15 cm periphery from the center along the long axis. The EP was used as an imitation of the human body with similar shape, size, and density, and was expected to cause scatter and CT number measurement error. CT scans were acquired after placement, into the holes of the phantoms, of micro test tubes filled with a dilution series of iodine contrast media. Iodine contrast media of 300 mg I/ml (iohexol, Omnipaque 300 Syringe; Daiichi Sankyo, Tokyo, Japan) was diluted by 5% to make a dilution equivalent to 15 mg I/ml iodine solution. Then twofold serial dilution was performed to make dilutions equivalent to 1.875, 3.75, and 7.5 mg I/ml iodine solution. Pure water was used as 0 mg I/ml solution.

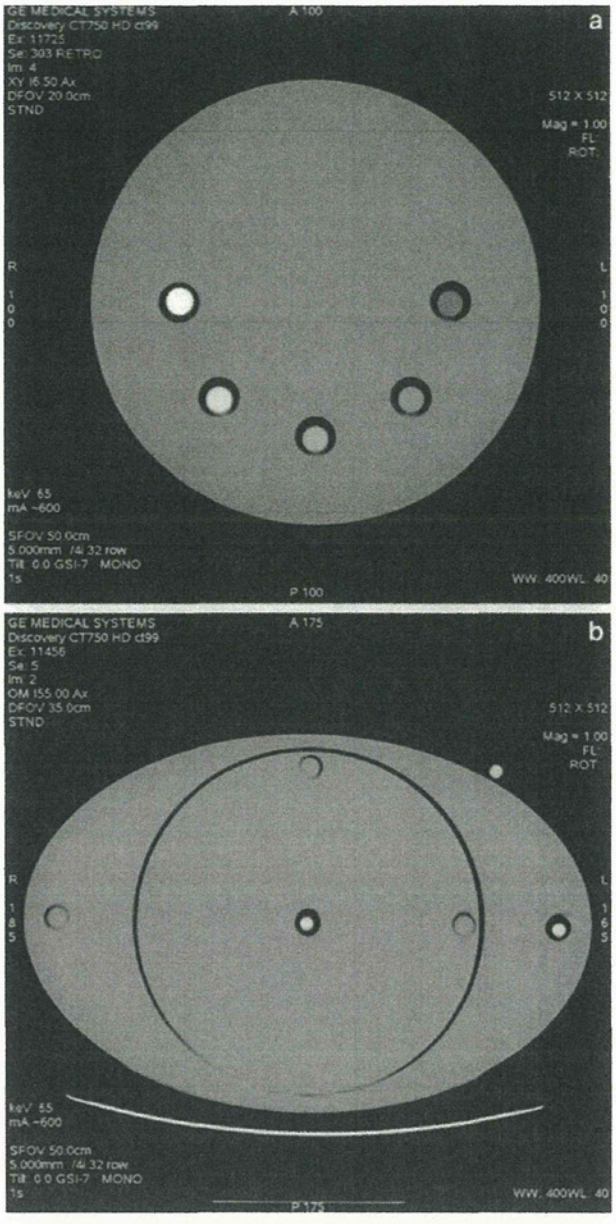

Fig. 1 **a** Simulated monochromatic CT image at 65 keV shows a sectional view of the circular phantom. The micro test tubes are filled with iodine contrast medium solutions at various concentrations. **b** Simulated monochromatic CT image at 65 keV shows a sectional view of the elliptical phantom. The *holes at the center* and at the 15 cm periphery along the *long axis* were used to evaluate the CT number of each solution of the iodine contrast media

CT imaging and measurement

Scans were acquired with a 64-slice CT system (Discovery CT 750HD; GE Healthcare). All examinations were performed in axial scanning mode with a large body filter. Conventional CT images were acquired with a tube potential of 120 kVp and tube current of 410 mA. Simulated monochromatic images at 65 keV were obtained by dual-energy CT spectral imaging

with fast kVp switching between 80 and 140 kVp, with a tube current of 600 mA. The tube current was set to adjust the volume computed tomography dose index ($CTDI_{vol}$) to a level similar to that in conventional CT. We chose a value of 65 keV for the simulated monochromatic images because CT numbers of water measured at 65 keV are similar to those measured in conventional imaging at tube potential of 120 kVp. Scanning was performed with the phantoms placed at the center of the scan field. The following parameters were used in both imaging techniques: detector coverage, 20 mm; slice thickness, 5.0 mm; rotation time, 1.0 s; scanned field-of-view, 50 cm. All images were reconstructed using STANDARD kernel with the target micro test tubes located at the center of the reconstructed image and a 20-cm field of view. Appropriate slices were selected to avoid partial volume effects at the ends of the tubes, and mean CT numbers were measured one time in HU using a circular region of interest (ROI) that was carefully placed at the center of the cross-sectional image of each tube. Area of the ROI was 20 mm^2, and the ROI was replicated with copy function on a workstation to measure all the tubes. $CTDI_{vol}$ values were recorded during CT scanning to evaluate radiation exposure.

Statistical analysis

A linear regression model was used to evaluate linearity. Variability of the CT numbers for each imaging method was investigated in terms of phantom shape using analysis of covariance with Bonferroni multiple-comparison correction. All statistical computations were performed using JMP software (version 8.0.2, SAS Institute Japan, Tokyo, Japan).

Results

Computed tomography numbers in HU corresponding to iodine concentration at 0, 1.875, 3.75, 7.5 and 15 mg I/ml were 2.31, 49.35, 99.84, 197.21 and 406.79, respectively, when using conventional image and the CP hole. Those for conventional image and the EP central and peripheral hole, and for simulated monochromatic image and the CP, EP central and peripheral hole were −2.67, 33.93, 77.10, 157.50 and 328.66; 1.11, 38.48, 84.97, 167.74 and 345.99; 2.22, 50.92, 103.49, 206.66 and 431.85; −2.08, 44.77, 95.98, 195.66 and 405.83; and 2.09, 46.49, 95.76, 198.35 and 413.55, respectively. Slopes of regression lines of the measured CT numbers for conventional image and the CP, EP central and peripheral hole, and simulated monochromatic image and the CP, EP central and peripheral hole were 27.01, 22.18, 23.10, 28.72, 27.27 and 27.61, respectively. There was a uniformly high correlation of CT number with iodine concentration, regardless of the combination of phantom and CT imaging method used (Table 1; Fig. 2). The coefficient of determination was above 0.999 under all experimental conditions.

In the conventional CT method, significant difference was found regarding the slope of the linear relation between CT number and concentration measured in the EP compared with those in the CP, although linearity was good for both phantoms, whereas no significant difference was found in measured slope for the simulated monochromatic images (Table 2). The mean CT numbers are presented in Table 1. The CT number for water density was approximately 0 HU (mean ± standard deviation, 0.50 ± 2.27) under all conditions.

$CTDI_{vol}$ values were 34.87 mGy for conventional CT and 36.18 mGy for dual-energy CT spectral imaging with fast kVp switching.

Discussion

Although both conventional and simulated monochromatic imaging achieved very high linearity of CT numbers in

Table 1 Measured CT numbers and regression parameters

Iodine concentration (mg I/ml)	Conventional-CP	Conventional-EP central	Conventional-EP peripheral	Simulated monochromatic-CP	Simulated monochromatic-EP central	Simulated monochromatic-EP peripheral
0	2.31	−2.67	1.11	2.22	−2.08	2.09
1.875	49.35	33.93	38.48	50.92	44.77	46.49
3.75	99.84	77.10	84.97	103.49	95.98	95.76
7.5	197.21	157.50	167.74	206.66	195.66	198.35
15	406.79	328.66	345.99	431.85	405.83	413.55
Regression parameters						
Slope	27.01	22.18	23.10	28.72	27.27	27.61
Y intercept	−0.83	−5.88	−2.27	−2.52	−5.38	−4.08
Coefficients of determination	0.9996	0.9996	0.9996	0.9993	0.9997	0.9992

CP circular phantom, *EP* elliptical phantom

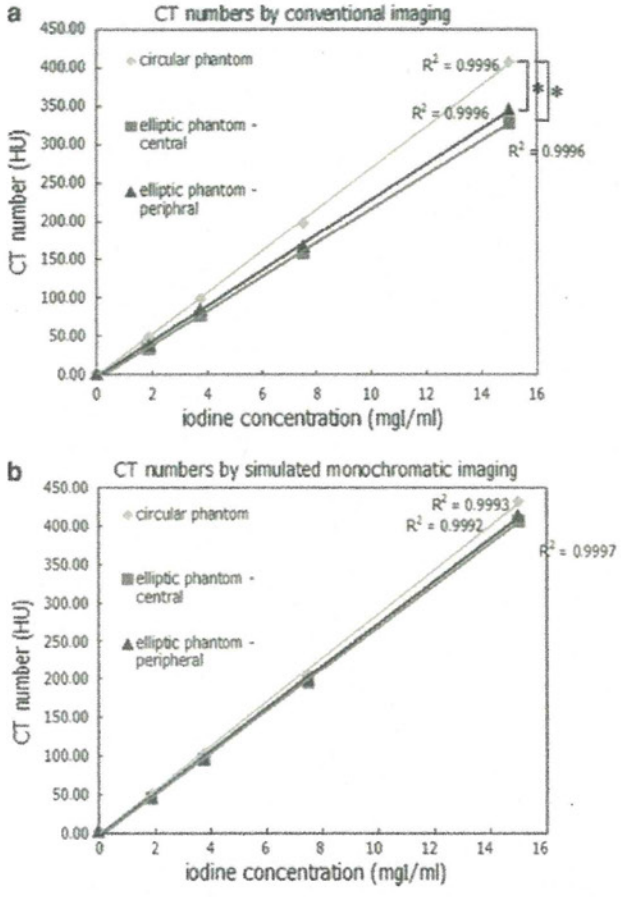

Fig. 2 **a** *Plots* of the CT numbers acquired with conventional CT imaging and their regression lines. All coefficients of determination (R^2) were above 0.999. The slopes of the regression lines calculated using the data from the center and the periphery of the elliptical phantom show a statistically significant difference compared with those of the circular phantom. **b** *Plots* of the CT numbers acquired with simulated monochromatic imaging using dual-energy CT and their regression lines. All coefficients of determination (R^2) were above 0.999. There was no statistically significant difference in slope among the three regression lines

terms of iodine concentration, consistent slopes were not attained in the conventional imaging method. Conventional imaging did not yield consistent CT numbers for the same iodine solution in differently shaped phantoms. In contrast, simulated monochromatic imaging produced almost the same CT numbers regardless of phantom shape. These results suggest that simulated monochromatic imaging using dual-energy spectral CT potentially enables better reproducibility of CT numbers, at least for iodine contrast media solutions, without influence from the surrounding environment.

It is possible that artifacts such as streaks could have affected the present results; however, none of the images acquired in our experiments demonstrated obvious undesirable artifacts. The very high linearity observed for all imaging methods and phantoms supports the assumption

Table 2 Comparisons of the slopes of CT numbers

	P value
Conventional imaging	
Circular versus elliptical central	<0.0001*
Circular versus elliptical peripheral	<0.0001*
Elliptical central versus elliptical peripheral	0.0482
Simulated monochromatic imaging	
Circular versus elliptical central	0.0281
Circular versus elliptical peripheral	0.1267
Elliptical central versus elliptical peripheral	0.5404

P values were calculated using analysis of covariance. $P < 0.0083$ was considered statistically significant with Bonferroni multiple-comparison correction

* Statistically significant

that focal artifacts do not cause slope inconsistency in conventional imaging; rather, a more diffuse variation of CT numbers exists that can be eliminated by using dual-energy CT imaging. In previously published papers, beam hardening has been frequently mentioned as a cause of pseudoenhancement [5–13]. When lower energy photons of the beam are preferentially attenuated by higher density material than water, and images are reconstructed with an algorithm that compensates the excessive attenuation, beam hardening occurs. Accuracy in CT number in our experiments using simulated monochromatic images was achieved at least partly because the beam-hardening effect was corrected with dual-energy measurements [17]. Additionally, in our experiment, CT number inconsistency was found in the measurements with EP that had similar size and density to the patient's body. Body-sized objects cause scatter and give rise to CT number measurement error, as Joseph et al. [19] demonstrated. Simulated monochromatic images might be accurate in CT number measurement because the error induced by scatter was compensated in the process of material decomposition, as Vetter et al. [20] indicated.

Clinically, increased attenuation of small simple renal cysts on contrast-enhanced CT is reported as 'pseudoenhancement;' however, enhancement of a renal mass on contrast-enhanced CT is an essential criterion for distinguishing between tumors and benign cysts [5–13]. The present results show the effect of the shape of surrounding tissue on the CT number of the lesion of interest. Essentially, variability in the shape of the surrounding tissue means that the distribution of density also varies. The density distribution in a contrast-enhanced CT image is substantially different from that in a plain CT image; one possible cause of pseudoenhancement may be this change in density distribution. The present results indicate that it may be possible to apply dual-energy CT to eliminate undesirable effects of the surrounding environment that

affect the CT number of the lesion of interest, to achieve accurate CT number acquisition. Furthermore, simulated monochromatic images created with dual-energy CT may enable more accurate diagnoses dependent on CT number measurement such as distinction between adrenal adenoma and other tumors [21–24] because the accuracy of CT number measurement without the influence of body shape means robustness against individual differences.

A potential disadvantage of dual-energy spectral CT is increased radiation exposure. In our experiment, however, the $CTDI_{vol}$ values for dual-energy CT spectral imaging were almost equivalent to conventional CT imaging. Although we did not assess image quality closely, standard deviation of background noise was below 10 HU in both the conventional and simulated monochromatic images. Both image sets seemed to show almost the same image quality subjectively. Simulated monochromatic images were capable of substituting for conventional CT images in this regard.

The present study has some limitations. We chose 65 keV as a parameter for simulated monochromatic imaging because these images have CT numbers similar to those of images acquired at 120 kVp in conventional imaging. However, we did not investigate optimal keV values for CT number reproducibility. In addition, this study was conducted as a phantom study, and clinical feasibility was not investigated.

The present results in a phantom study demonstrated that CT number consistency was better achieved by dual-energy spectral CT imaging than by conventional CT imaging. This result has some possible practical applications in clinical CT. Using the dual-energy spectral CT imaging method, precise measurement of CT number could be obtained, thereby enabling more accurate comparison of the densities of lesions of interest. In conclusion, the measured CT attenuation numbers of water solutions of iodine contrast media varied depending on phantom shape, and dual-energy CT spectral imaging using simulated monochromatic images achieved better CT number consistency than that obtained using conventional CT imaging.

Acknowledgments We gratefully acknowledge Kosuke Sasaki, M.S., and Koji Segawa, R.T., for their technical support and assistance in data acquisition.

References

1. Levi C, Gray J, McCullough E, Hattery R. The unreliability of CT numbers as absolute values. Am J Roentgenol. 1982;139: 443–7.
2. Zerhouni EA, Spivey JF, Morgan RH, Leo FP, Stitik FPa, Siegelman SS. Factors influencing quantitative CT measurements of solitary pulmonary nodules. J Comput Assist Tomogr. 1982;6: 1075–87.
3. McCullough E, Morin R. CT-number variability in thoracic geometry. Am J Roentgenol. 1983;141:135–40.
4. Birnbaum BA, Hindman N, Lee J, Babb JS. Multi-detector row CT Attenuation measurements: assessment of intra- and interscanner variability with an anthropomorphic body CT phantom. Radiology. 2007;242:109–19.
5. Maki DD, Birnbaum BA, Chakraborty DP, Jacobs JE, Carvalho BM, Herman GT. Renal cyst pseudoenhancement: beam-hardening effects on CT numbers. Radiology. 1999;213: 468–72.
6. Coulam CH, Sheafor DH, Leder RA, Paulson EK, DeLong DM, Nelson RC. Evaluation of pseudoenhancement of renal cysts during contrast-enhanced CT. Am J Roentgenol. 2000;174:493–8.
7. Bae KT, Heiken JP, Siegel CL, Bennett HF. Renal cysts: is attenuation artifactually increased on contrast-enhanced CT images? Radiology. 2000;216:792–6.
8. Birnbaum BA, Maki DD, Chakraborty DP, Jacobs JE, Babb JS. Renal cyst pseudoenhancement: evaluation with an anthropomorphic body CT phantom. Radiology. 2002;225:83–90.
9. Abdulla C, Kalra MK, Saini S, Maher MM, Ahmad A, Halpern E, et al. Pseudoenhancement of simulated renal cysts in a phantom using Different multidetector CT scanners. Am J Roentgenol. 2002;179:1473–6.
10. Heneghan JP, Spielmann AL, Sheafor DH, Kliewer MA, DeLong DM, Nelson RC. Pseudoenhancement of simple renal cysts: a comparison of single and multidetector helical CT. J Comput Assist Tomogr. 2002;26:90–4.
11. Israel GM, Bosniak MA. Pitfalls in renal mass evaluation and how to avoid them. Radiographics. 2008;28:1325–38.
12. Birnbaum BA, Hindman N, Lee J, Babb JS. Renal cyst pseudoenhancement: influence of multidetector CT reconstruction algorithm and scanner type in phantom model. Radiology. 2007; 244:767–75.
13. Wang ZJ, Coakley FV, Fu Y, Joe BN, Prevrhal S, Landeras LA, et al. Renal cyst pseudoenhancement at multidetector CT: what are the effects of number of detectors and peak tube voltage? Radiology. 2008;248:910–6.
14. Graser A, Johnson TRC, Bader M, Staehler M, Haseke N, Nikolaou K, et al. Dual energy CT characterization of urinary calculi: initial in vitro and clinical experience. Invest Radiol. 2008;43:112–9.
15. Boll DT, Patil NA, Paulson EK, Merkle EM, Simmons WN, Pierre SA, et al. Renal stone assessment with dual-energy multidetector CT and advanced postprocessing techniques: improved characterization of renal stone composition—pilot study. Radiology. 2009;250:813–20.
16. Thomas C, Patschan O, Ketelsen D, Tsiflikas I, Reimann A, Brodoefel H, et al. Dual-energy CT for the characterization of urinary calculi: in vitro and in vivo evaluation of a low-dose scanning protocol. Eur Radiol. 2009;19:1553–9.
17. Alvarez RE, Macovski A. Energy-selective reconstruction in X-ray computerized tomography. Phys Med Biol. 1976;21: 733–44.
18. Wu X, Langan DA, Xu D, Benson TM, Pack JD, Schmitz AM, et al. Monochromatic CT image representation via fast switching dual kVp. In: Proceedings of the SPIE, vol. 7258; 2009. p. 725845.
19. Joseph PM, Spital RD. The effects of scatter in X-ray computed tomography. Med Phys. 1982;9:464–72.
20. Vetter JR, Holden JE. Correction for scattered radiation and other background signals in dual-energy computed tomography material thickness measurements. Med Phys. 1988;15:726–31.
21. van Erkel AR, van Gils AP, Lequin M, Kruitwagen C, Bloem JL, Falke TH. CT and MR distinction of adenomas and non-adenomas of the adrenal gland. J Comput Assist Tomogr. 1994; 18:432–8.

22. McNicholas MM, Lee MJ, Mayo-Smith WW, Hahn PF, Boland GW, Mueller PR. An imaging algorithm for the differential diagnosis of adrenal adenomas and metastases. Am J Roentgenol. 1995;165:1453–9.
23. Miyake H, Takaki H, Matsumoto S, Yoshida S, Maeda T, Mori H. Adrenal nonhyperfunctioning adenoma and nonadenoma: CT attenuation value as discriminative index. Abdom Imaging. 1995;20:559–62.
24. Korobkin M, Brodeur FJ, Yutzy GG, Francis IR, Quint LE, Dunnick NR, et al. Differentiation of adrenal adenomas from nonadenomas using CT attenuation values. Am J Roentgenol. 1996;166:531–6.

Jpn J Radiol (2012) 30:146–153
DOI 10.1007/s11604-011-0026-7

ORIGINAL ARTICLE

Effect of radiation dose and adaptive statistical iterative reconstruction on image quality of pulmonary computed tomography

Jiro Sato · Masaaki Akahane · Sachiko Inano · Mariko Terasaki · Hiroyuki Akai · Masaki Katsura · Izuru Matsuda · Akira Kunimatsu · Kuni Ohtomo

Received: 3 July 2011 / Accepted: 1 October 2011 / Published online: 17 December 2011

Abstract
Purpose The purpose of this study was to assess the effects of dose and adaptive statistical iterative reconstruction (ASIR) on image quality of pulmonary computed tomography (CT).
Materials and methods Inflated and fixed porcine lungs were scanned with a 64-slice CT system at 10, 20, 40 and 400 mAs. Using automatic exposure control, 40 mAs was chosen as standard dose. Scan data were reconstructed with filtered back projection (FBP) and ASIR. Image pairs were obtained by factorial combination of images at a selected level. Using a 21-point scale, three experienced radiologists independently rated differences in quality between adjacently displayed paired images for image noise, image sharpness and conspicuity of tiny nodules. A subjective quality score (SQS) for each image was computed based on Anderson's functional measurement theory. The standard deviation was recorded as a quantitative noise measurement.
Results At all doses examined, SQSs improved with ASIR for all evaluation items. No significant differences were noted between the SQSs for 40%-ASIR images obtained at 20 mAs and those for FBP images at 40 mAs.
Conclusion Compared to the FBP algorithm, ASIR for lung CT can enable an approximately 50% dose reduction from the standard dose while preserving visualization of small structures.

Keywords Computed tomography · Iterative reconstruction · Dose reduction · Image quality

J. Sato (✉) · M. Akahane · S. Inano · M. Terasaki · H. Akai · M. Katsura · I. Matsuda · A. Kunimatsu · K. Ohtomo
Department of Radiology, Graduate School of Medicine, The University of Tokyo, 7-3-1 Hongo, Bunkyo-ku, Tokyo 113-8655, Japan
e-mail: jsato-tky@umin.ac.jp

M. Akahane
e-mail: akahane-tky@umin.ac.jp

S. Inano
e-mail: dzsachi@hotmail.com

M. Terasaki
e-mail: hasimari-1101@hotmail.co.jp

H. Akai
e-mail: commonhiro@hotmail.com

M. Katsura
e-mail: mskktsr@gmail.com

I. Matsuda
e-mail: imatsudajp@yahoo.co.jp

A. Kunimatsu
e-mail: akrk-tky@umin.ac.jp

K. Ohtomo
e-mail: kotomo-tky@umin.ac.jp

Introduction

Worldwide, the number of CT examinations has escalated from one to three procedures per 1000 people during 1977–1980 to about 35 procedures per 1000 people during 1997–2007 [1]. CT accounts for more than 40% of the collective effective dose of medical radiation worldwide [1], and 0.6–3.2% of the cumulative risk of cancer until the age of 75 could be attributable to diagnostic exposure in developed countries [2]. Thus, public concerns about medical radiation exposure and dose reduction have been growing. Reducing the dose, however, results in an increase in image noise that degrades image quality with the standard filtered back projection (FBP) reconstruction. Some image filters can reduce noise, but use of them tends